**Title**
Estimates of Hadronic Backgrounds in a 5 TeV e+e- Linear Collider



**Author**
Ohgaki, Tomomi

**Publication Date**
1998-07-01

LBNL-42433

# Estimates of Hadronic Backgrounds in a 5 TeV $e^+e^-$ Linear Collider

T. Ohgaki*, M. Xie*, and H. Murayama†

*†*Lawrence Berkeley National Laboratory, Berkeley, California 94720*
*† University of California, Berkeley, California 94720*

**Abstract.** We have estimated hadronic backgrounds by $\gamma\gamma$ collisions in an $e^+e^-$ linear collider at a center-of-mass energy of 5 TeV. We introduce a simple ansatz, that is, a total $\gamma\gamma$ cross section of $\sigma_{\gamma\gamma} = (\sigma_{\gamma p})^2/\sigma_{pp}$ shall be saturated by minijet productions, whose rate is controlled by $p_{t,min}(\sqrt{s})$. We present that the background yields are small and the energy deposits are tinier than the collision energy of the initial electron and positron beams by a simulation.

## I INTRODUCTION

A combination of beamstrahlung and 'strong' QCD interactions of the photon can induce hadronic backgrounds at future $e^+e^-$ linear colliders. An operation of the $e^+e^-$ linear collider at 5 TeV center-of-mass energy beyond the Large Hadron Collider and the 500 GeV $e^+e^-$ linear collider requires a luminosity of $10^{35}\mathrm{cm}^{-1}\mathrm{s}^{-1}$ for a study of particle physics. In order to achieve the required luminosity in several TeV colliders, we need to more strongly focus the electron and positron beams at the interaction point. In the circumstance, a large number of beamstrahlung photons are radiated due to the collective electromagnetic field of the oncoming beam bunch. Some of collisions between them convert to $e^+e^-$ pairs and others generate hadrons.

At high energy, we can consider that the photon consists of the partons which are quarks and gluons, and the interactions among the partons in two-photon collisions can be calculated using perturbative QCD. The experiments at TRISTAN, first indicated that the jet production in two-photon interactions were dominated by the resolved processes [1,2]. Drees and Godbole [3] called attention to the minijet backgrounds for future $e^+e^-$ linear colliders, because the cross section of minijets, by the calculation method of the parton-parton scattering, rises very fast with energy. Recently, two measurements of $\gamma\gamma$ collisions at the CERN $e^+e^-$ collider LEP exhibit the rising of the total cross section for $\gamma\gamma \to hadrons$ with energy [4,5]. The minijet cross sections for description of hadronic events have uncertainties at

several TeV energy, related to the cutoff of transverse momentum of the jet, $p_{t,min}$, such as a free parameter. Below $p_{t,min}$, the perturbative QCD calculations fail altogether and the transition region between hard and soft processes is not well defined. In addition, the parton density functions of the photon for the minijet cross section are parameterized according to the experimental data at low energies. In consequence, we can not simply estimate the number of hadronic events in 5 TeV $e^+e^-$ linear colliders by using these cross sections [6,7].

In general, $\gamma\gamma$ interactions are similar to hadron-hadron interactions at high energy. The total cross sections for $pp$ and $\gamma p$ collisions have been measured at several TeV and hundreds GeV, which are more larger than $\gamma\gamma$ experimental data, respectively [8] and are well described by the Regge theorem [9]. We propose therefore the simple model by taking a phenomenological approach. First, the cross section for $\gamma\gamma$ collisions by the factorization theorem $\sigma_{\gamma\gamma} = (\sigma_{\gamma p})^2/\sigma_{pp}$ [10,11] is applied and we estimate the number of hadronic events at a 5 TeV $e^+e^-$ linear collider. Next, the simple ansatz, that the total cross section of $\gamma\gamma$ minijets is supposed as that for $\gamma\gamma$ collisions, is applied and we compute the spatial distribution for $\gamma\gamma$ minijets. The detailed information of the minijets from realistic simulations is used to remove the hadronic backgrounds effectively.

Until now the hadron production in $\gamma\gamma$ collisions as a backgrounds for $e^+e^-$ linear colliders at $\sqrt{s}_{e^+e^-}$=0.5 and 1.0 TeV has been studied [1,10,12]. Recently the design study for 5 TeV linear colliders based on laser acceleration has been started and it presents that the effects of quantum suppression of beamstrahlung due to the very short bunch length are effective [13,14]. In sec. 2, we calculate the luminosity distribution of $\gamma\gamma$ collisions at a 5 TeV $e^+e^-$ linear collider based on laser acceleration. In sec. 3, we describe the factorization theorem about the cross section for $\gamma\gamma$ collisions and the simple ansatz of $\gamma\gamma$ minijets. In sec. 4 we estimate hadronic backgrounds by $\gamma\gamma$ collisions by a simulation.

## II LUMINOSITY DISTRIBUTION OF A 5 TEV LINEAR COLLIDER

We will describe the spectrum of photon-photon luminosity in a 5 TeV $e^+e^-$ linear collider. There are two processes for $\gamma\gamma$ collisions in $e^+e^-$ colliders. Beamstrahlung is a synchrotron radiation induced by the collective fields of the oncoming colliding beams. The average Upsilon parameter in a linear collider [15], which expresses the dependence of the beamstrahlung spectrum, is $\Upsilon = \frac{5}{6}\frac{N_e r_e^2 \gamma}{\alpha\sigma_z(\sigma_x+\sigma_y)}$, where $\alpha$ is the fine structure constant, $N_e$ the number of particles per bunch, $r_e$ the classical electron radius, $\gamma$ the Lorentz factor of the beam, $\sigma_z$ the rms bunch length, and $\sigma_x, \sigma_y$ the transverse and vertical sizes of the bunch at the interaction point. In this paper, we use the beamstrahlung spectrum in the regime $\Upsilon \gg 1$, taking advantage of effects of quantum suppression of beamstrahlung [13,14]. The spectra of beamstrahlung photons in the high $\Upsilon$ regime was calculated by the numerical computation [16]. In order to perform more realistic calculation including disruption and multiple

beamstrahlung effects, we have simulated the luminosity distribution by using the CAIN code, which is a Monte Carlo program of the beam-beam interactions in future linear colliders [17].

Bremsstrahlung photons are emitted by the collisions of individual particles. The bremsstrahlung spectrum from electron beams is given by the well-known equivalent photon approximation [12]

$$f_{\gamma,e}(y) = \frac{\alpha}{2\pi}\left(\frac{1+(1-y)^2}{y}\ln\left[\frac{(1-y)}{m_e^2 y^2}P_{\max}^2\right] - \frac{2(1-y)}{y}\right), \qquad (1)$$

where $y$ and $P_{\max}^2$ denote the energy fraction taken by the photon from the electron and the maximum photon virtuality. $m_e$ is the electron mass. In this article the photon virtuality was restricted to $P_{\max}^2 = 0.01$ GeV$^2$ [12].

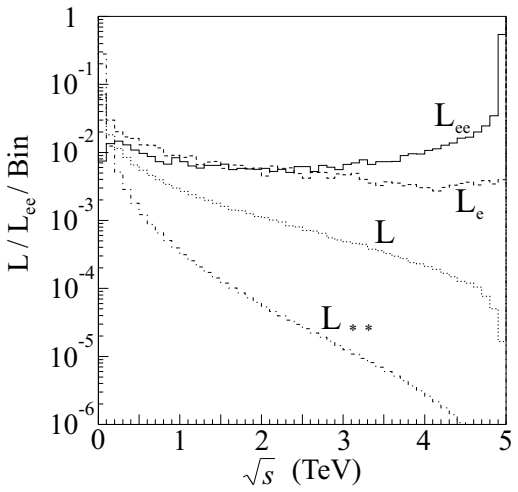


**FIGURE 1.** Luminosity distribution of a 5 TeV $e^+e^-$ linear collider with $\Upsilon = 631$. The vertical axis is normalized by the total luminosity of the $e^+e^-$ collisions. The bin size is 100 GeV.

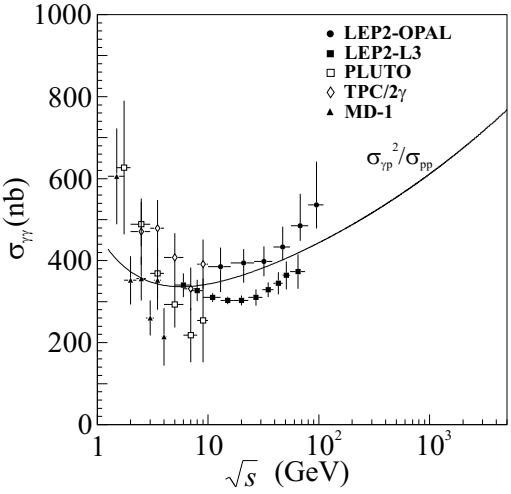


**FIGURE 2.** The experimental data of the total cross section of $\gamma\gamma$ collisions. The measurements by PLUTO, TPC/2$\gamma$, MD1, L3, and OPAL are shown [4,5,18]. The data are compared to $(\sigma_{\gamma p})^2/\sigma_{pp}$.

**TABLE 1.** Beam parameters of an $e^+e^-$ linear collider with the laser drive at $\sqrt{s}_{e^+e^-}$=5 TeV [13].

| $\Upsilon$ | $P_b$ (MW) | $N_e(10^8)$ | $f_c$ (kHz) | $\epsilon_x/\epsilon_y$ (nm) | $\beta_x/\beta_y(\mu$m) | $\sigma_x/\sigma_y$ (nm) | $\sigma_z$ ($\mu$m) |
|---|---|---|---|---|---|---|---|
| 631 | 20 | 1.6 | 156 | 25/25 | 62/62 | 0.56/0.56 | 1 |

The beam parameters of an $e^+e^-$ linear collider with the laser drive at $\sqrt{s}_{e^+e^-} = 5$ TeV are listed in Table 1. The $\Upsilon$ parameter of the laser-driven $e^+e^-$ collider is some hundreds, because $\sigma_z$ is much smaller than that of conventional microwaves due to

**TABLE 2.** Total luminosity of an $e^+e^-$ linear collider with the laser drive at $\sqrt{s}_{e^+e^-}$=5 TeV (Unit $10^{35}\mathrm{cm}^{-2}\mathrm{s}^{-1}$).

| | $L_{ee}$ | $L_{e\gamma}$ | $L_{\gamma\gamma}$ | $L_{\gamma^*\gamma^*}$ |
|---|---|---|---|---|
| Total | 1.25 | 0.491 | 0.209 | 0.386 ($\sqrt{s}$ >0.1 TeV) |
| $\sqrt{s}$ >4.975 TeV | 0.606 | $6.28\times10^{-4}$ | $4.91\times10^{-7}$ | $1.80\times10^{-9}$ |

the typical wavelength of accelerating wakefield for laser wakefield acceleration, which is about 100 $\mu$m.

Figure 1 shows the luminosity distribution of a 5 TeV linear collider with $\Upsilon = 631$. The luminosity distribution of the $e^+e^-$, $e\gamma$, and $\gamma\gamma$ collisions in Fig. 1 have been calculated by using the CAIN code. That of the $\gamma^*\gamma^*$ collisions ($\gamma^*$ denotes virtual photons.) was calculated by $L_{\gamma^*\gamma^*}(\sqrt{s}) = L_{ee}\int_0^1\int_0^1 f_{\gamma,e}(y_1)f_{\gamma,e}(y_2)\delta\left(s-4y_1y_2E_e^2\right)dy_1dy_2$, where $E_e$ is the energy of initial electrons, using the analytic formula of Eq.(1). It is needless to say that we will have to consider the superposition of the beamstrahlung and bremsstrahlung spectrums.

The total luminosity of an $e^+e^-$ linear collider with the laser drive at $\sqrt{s}_{e^+e^-} = 5$ TeV are listed in Table 2. There is about a half of the total luminosity of the $e^+e^-$ collisions with $\sqrt{s} > 4.975$ TeV and it presents a narrow width for precision study. The maximum energy of the collisions between beamstrahlung photons reaches near $\sqrt{s} = 5$ TeV due to the large $\Upsilon$ parameter. The collisions between bremsstrahlung photons over $\sqrt{s} > 1$ TeV is negligible in comparison with other collisions.

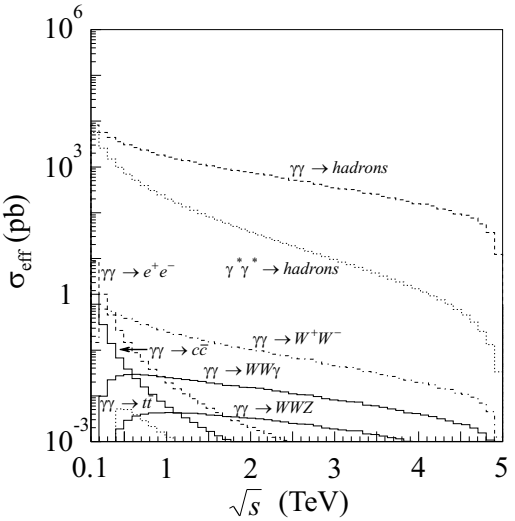


**FIGURE 3.** The effective cross section of the $\gamma\gamma$ collisions.

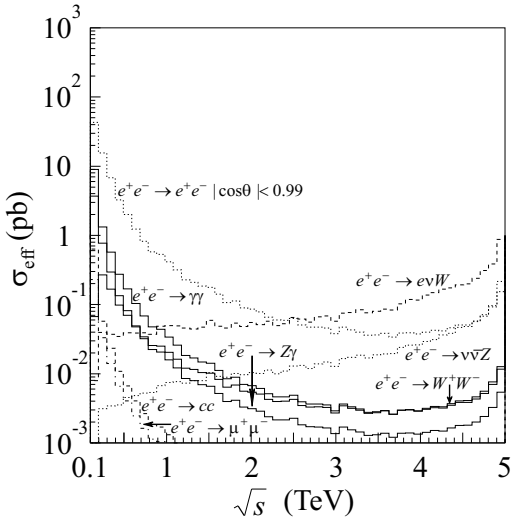


**FIGURE 4.** The effective cross section of the $e^+e^-$ collisions.

# III THE CROSS SECTION OF $\gamma\gamma$ MINIJETS

## A The total cross section of $\gamma\gamma$ collisions

In general, $\gamma\gamma$ interactions are similar to hadron-hadron interactions at high energy. The total cross sections for $pp$ and $\gamma p$ collisions [8] are well described by the Regge parameterization $\sigma = Xs^{\epsilon} + Ys^{-\eta}$ [9]

$$\sigma_{\gamma p} = 0.071\ s^{0.075} + 0.12\ s^{-0.46}\ \text{mb}, \tag{2}$$

$$\sigma_{pp} = 22.0\ s^{0.079} + 56.1\ s^{-0.46}\ \text{mb}, \tag{3}$$

where $\sqrt{s}$ is the center-of-mass energy of the interaction and is given in GeV. The experimental data of $pp$ collisions have been measured over $\sqrt{s} = 1$ TeV and the HERA measurements at DESY $ep$ collider have accumulated the $\gamma p$ collisions at near $\sqrt{s} = 200$ GeV. The formulas Eq.(2) and (3) accommodates with these data. The ratio of $\sigma_{\gamma p}/\sigma_{pp}$ is about 0.003 except for $\sqrt{s} < 10$ GeV and it presents that the behavior of $\gamma p$ interactions at center-of-mass energies is similar to that of $pp$ interactions. Therefore we adopt the following factorization theorem [10,11]

$$\frac{\sigma_{\gamma\gamma}}{\sigma_{\gamma p}} = \frac{\sigma_{\gamma p}}{\sigma_{pp}}, \tag{4}$$

where $\sigma_{\gamma\gamma}$ is the total cross section for $\gamma\gamma$ collisions.

The experimental data of the total cross section of $\gamma\gamma$ collisions [4,5,18] are shown in Fig. 2. The observed energy dependence of the cross section of the L3 and OPAL measurements is similar, but the OPAL values are about 20% higher [5]. In this figure the data are compared to $\sigma_{\gamma\gamma} = (\sigma_{\gamma p})^2/\sigma_{pp}$ and the $\sigma_{\gamma\gamma}$ gives a reasonable description of the total cross section of $\gamma\gamma$ collisions.

In order to contrast the processes of $\gamma\gamma \to hadrons$ with the other processes in the standard model, we present the effective cross section of $\gamma\gamma$ collisions in Fig. 3. The effective cross section is obtained by $\sigma_{\text{eff}}(\sqrt{s}) = \frac{\sigma(\sqrt{s})}{L_{total}} \frac{dL}{d\sqrt{s}}|_{\sqrt{s}}$, and we can get easily the number of events by multiplying it by the amount of the luminosity. Here the total cross sections for the other processes in the standard model were calculated by the CompHEP and GRACE codes [19,20]. The $\gamma\gamma$ luminosity except for $\gamma^*\gamma^* \to hadrons$ originate from beamstrahlung photons. The effective cross section of $\gamma\gamma \to hadrons$ from beamstrahlung photons is about $10^4$ times larger than that of $\gamma\gamma \to W^+W^-$. When the collision energy is increasing, the effective cross sections of $\gamma\gamma$ collisions are almost decreasing.

Figure 4 and 5 show the effective cross section of $e^+e^-$ and $e\gamma$ collisions. At 5 TeV, the processes of $e^+e^- \to e\nu W, \nu\bar{\nu}Z, e^+e^-(|\cos\theta| < 0.99)$ and $e\gamma \to W\nu$ are dominant as well as $\gamma\gamma \to hadrons$. Especially the events of $e^+e^- \to e\nu W$ is comparable to those of $\gamma\gamma \to hadrons$ at 5 TeV.

Figure 6 shows the events of $\gamma\gamma$ minijets per bunch crossing. Number of events of $\gamma\gamma$ minijets per bunch crossing are listed in Table 3. From the figure and table,

the hadronic backgrounds from bremsstrahlung photons are small at TeV energy as compared with those from beamstrahlung photons with $\Upsilon = 631$. The probability to have an event without background is $P_{clean} \equiv e^{-<n>}$. Here $< n >$ is the average number of background events. When $< n >= 1.62 \times 10^{-2}$ from collisions between beamstrahlung photons in the range 1 TeV $< \sqrt{s} <$ 5 TeV in the table, $P_{clean} =$ 0.984. It presents that the number of hadronic backgrounds per bunch crossing is small so that it will not affect the performance of the detection in a study of particle physics. The number of events per bunch is inversely proportional to the collision frequency, because the luminosity per bunch is $L_{bunch} = L_{total}/f_c$. In this paper, the collision frequency of 5 TeV $e^+e^-$ linear collider with the laser drive is 156 kHz and is higher than the frequency $120 \times 225$ Hz with 34 GHz normal conducting RF [21]. Until now the bunch scheme of the laser-driven linear collider is not well studied. We further need to estimate the number of hadronic backgrounds taking account of the bunch scheme of the laser-driven linear colliders.

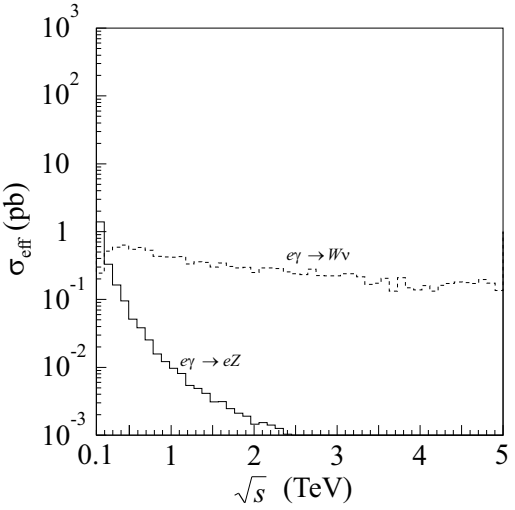


**FIGURE 5.** The effective cross section of the $e\gamma$ collisions.

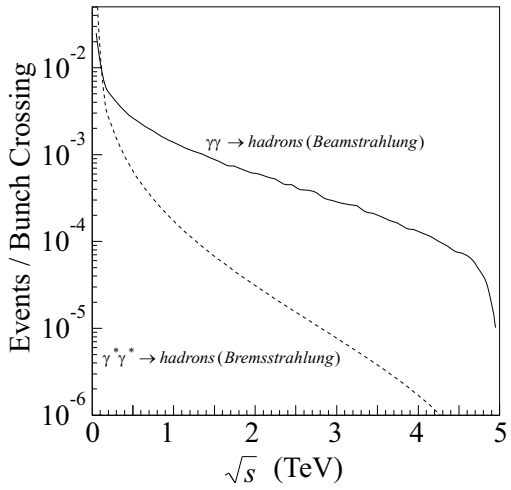


**FIGURE 6.** The events of $\gamma\gamma$ minijets per bunch crossing.

**TABLE 3.** Number of events of $\gamma\gamma$ minijets per bunch crossing.

| Energy range | Beamstrahlung | Bremsstrahlung |
|---|---|---|
| 1 GeV$< \sqrt{s} <$5 TeV | $6.85 \times 10^{-2}$ | $1.14 \times 10^{-1}$ |
| 1 TeV$< \sqrt{s} <$5 TeV | $1.62 \times 10^{-2}$ | $9.95 \times 10^{-4}$ |

## B The differential cross section of $\gamma\gamma$ minijets

A real photon has a complicated nature, $\gamma\gamma$ events are divided into several event classes by the combinations of the nature of the two incoming photons [22]. The total cross section for $\gamma\gamma$ collisions is divided by

$$\sigma_{\gamma\gamma} = \sigma_{minijets} + \sigma_{\rm soft-VMD} = \int_{p_{t,min}}^{\infty} \frac{d\sigma_{minijets}}{dp_t}\, dp_t + \sigma_{\rm soft-VMD}, \tag{5}$$

where $\sigma_{minijets}$ is the total cross section of $\gamma\gamma$ minijets. In lowest order, the minijet events consist of the 'direct' process $\gamma\gamma \to q\bar{q}$, the '1-resolved' processes $\gamma q \to qg$ and $\gamma \mathrm{g} \to \mathrm{q\bar{q}}$, and the '2-resolved' processes $qq' \to qq', q\bar{q}' \to q\bar{q}', q\bar{q} \to q'\bar{q}', q\bar{q} \to \mathrm{gg}, \mathrm{qg} \to \mathrm{qg}, \mathrm{gg} \to \mathrm{q\bar{q}}$, and $\mathrm{gg} \to \mathrm{gg}$. In general, the minijet cross section is infrared divergent and requires a cutoff at low transverse momentum. $\sigma_{\rm soft-VMD}$ is the total cross section of the soft vector meson dominance (VMD) events which are the elastic, diffractive and low-$p_t$ events at $p_t < p_{t,min}$. At higher energies, the soft-VMD events are more smaller than the minijet events [22] and the $\gamma\gamma$ minijet events with high $p_t$ dominate in $\gamma\gamma$ hadronic events.

We simply summarize the cross section of the $\gamma\gamma$ minijets [3,23,24]. In leading order(LO), the differential cross section for $\gamma\gamma$ minijets of two (partonic) jets with transverse momentum $p_t$ and (pseudo) rapidities $\eta_1, \eta_2$ can be written as [24]

$$\frac{d^3\sigma_{minijets}(\gamma\gamma \to j_1 j_2 X)}{dp_t d\eta_1 d\eta_2} = 2p_t x_1 x_2 \sum_{i,j,k,l} f_{i|\gamma}(x_1) f_{j|\gamma}(x_2) \frac{d\hat{\sigma}_{ij\to kl}\left(\hat{s},\hat{t},\hat{u}\right)}{d\hat{t}}, \tag{6}$$

where $i$ or $j$ is a photon, quark or gluon, and $k$ or $l$ is a quark or gluon. Here $f_{i|\gamma}$ is the parton density function of the photon. If $i = \gamma$ (direct contribution), the function $f_{i|\gamma}$ is unity. $x$ is the fraction of the jet energy carried by the parton in the photon. The subprocess cross sections $\hat{\sigma}$ for the direct and resolved photon contributions depend on the Mandelstam variables describing the hard partonic scattering, $\hat{s} = x_1 x_2 s$ and $\hat{t}$ [24].

In order to grasp the behavior of the total cross section of $\gamma\gamma$ minijets at higher energies, we have computed several cross sections by the PDFLIB 7.09 [25] and PYTHIA 5.7 [26] codes. These total cross sections can be calculated including higher order effects by using the Monte Carlo codes. Figure 7 shows the cross sections of $\gamma\gamma$ minijets. The parton density functions DG-G [27], LAC-1 [28], GS-G [29], AFG-G [30], and SaS-G 2M [31] have been calculated with $p_{t,min}$=2 GeV except for the function GRV-G [32] with $p_{t,min}$=3 GeV. The cross sections are compared to Chen's model [10] with $p_{t,min}$=3.2 GeV. The results of this figure show that the total cross sections of minijets almost rise very fast and are large at 5 TeV collision energy. It is known as the saturation problem of the photon density function at higher energies [6], and its problem does not depend on the parameterizations of the photon density function. Moreover the difference between the cross sections at higher energies greatly depend on the choice of $p_{t,min}$, such

as a free parameter. Therefore we do not simply accept the number of the events of these minijet cross sections. After we introduce the simple ansatz for the cross section of $\gamma\gamma$ minijets.

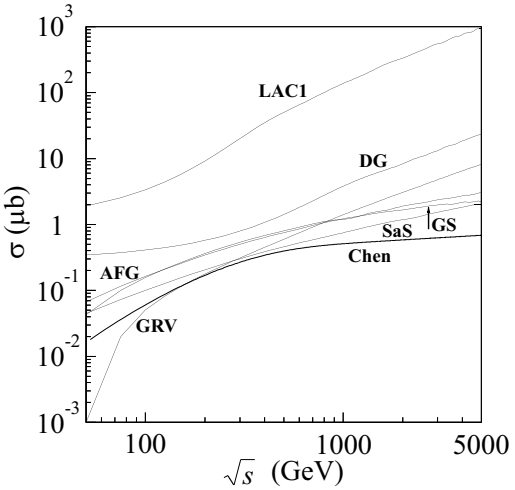


**FIGURE 7.** The cross sections of $\gamma\gamma$ minijets. Computed by the PDFLIB 7.09 [25] and PYTHIA 5.7 [26] codes. The parton density functions have been calculated with $p_{t,min}$ = 2 GeV except for the function GRV-G with $p_{t,min}$ = 3 GeV. The cross sections are compared to Chen's model [10] with $p_{t,min}$ = 3.2 GeV.

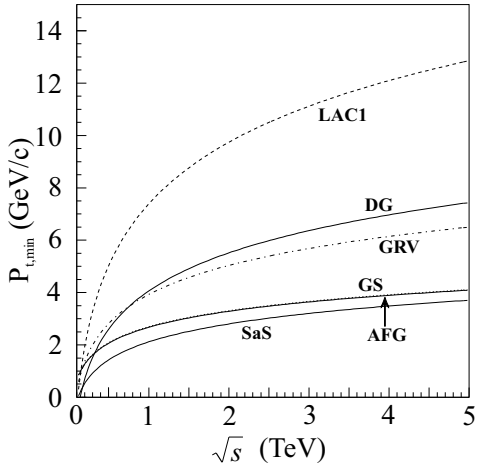


**FIGURE 8.** The minimum of the transverse momentum $p_{t,min}$ which depends on the parton density function of the photon.

In order to evaluate the spatial distribution from minijet events, we must define the differential cross section of $\gamma\gamma$ minijets. Previously we have assumed the total cross section of $\gamma\gamma$ collisions as $(\sigma_{\gamma p})^2/\sigma_{pp}$. Now we can not rely on the total cross sections of $\gamma\gamma$ minijets calculated by present parton density functions of the photon at higher energies. Therefore we consider $(\sigma_{\gamma p})^2/\sigma_{pp}$ as the upper bound of the minijet cross section. We obey this simple ansatz and the total cross section of $\gamma\gamma$ minijets is defined by

$$\sigma_{minijets}(p_{t,min}(\sqrt{s})) = \int_{p_{t,min}}^{\infty} \frac{d\sigma_{minijets}}{dp_t}\, dp_t \equiv \sigma_{\gamma p}^2/\sigma_{pp}. \tag{7}$$

To satisfy the equality in Eq.(7), we change the parameter $p_{t,min}(\sqrt{s})$ according to each parton density function of the photon. The minimum of the transverse momentum $p_{t,min}$ is defined as

$$p_{t,min}(\sqrt{s}) = a \ln \sqrt{s/b}, \tag{8}$$

where $a$ and $b$ are the fitting coefficients given in GeV and $(\mathrm{GeV})^2$.

**TABLE 4.** The fitting coefficients $a$ and $b$ of the minimum of the transverse momentum $p_{t,min}$ which depends on the parton density function of the photon. There are the sets of leading order (LO) and next-to-leading order (NLL) evolutions.

| Parton Density Function | Order of $\alpha_s$ | a (GeV) | b $(\text{GeV})^2$ |
|---|---|---|---|
| DG-G Set 1 | LO | 2.1 | 21000 |
| LAC-G Set 1 | LO | 3.4 | 13000 |
| GS-G-96 HO | NLL | 0.88 | 2200 |
| GRV-G | LO | 1.6 | 7400 |
| AFG-G Set HO | NLL | 0.88 | 2300 |
| SaS-G 2M | LO | 0.99 | 14000 |

Table 4 lists the fitting coefficients $a$ and $b$ of the minimum of the transverse momentum $p_{t,min}$ which depends on each parton density function of the photon. The $p_{t,min}$ of the GS-G parameterization is similar to that of AFG-G in the table. The minimum of the transverse momentum $p_{t,min}$ which depends on the parton density function of the photon are presented in Fig. 8. The LAC-1 parameterization is larger than others and about 13 GeV at $\sqrt{s}$=5 TeV. In the following section, we use the $p_{t,min}$ for estimation of hadronic backgrounds.

# IV RESULTS OF SIMULATION

In the previous section, we have estimated the number of minijet backgrounds per bunch crossing, but the number relies on the simple ansatz and the bunch scheme of the laser-driven linear colliders is not well-known. If we grasp the spatial distribution of $\gamma\gamma$ minijets, we can remove the hadronic backgrounds effectively. By the detailed information of the visible energy and the transverse momentum, and so on of the jets from realistic simulations, we can reach near the probability $P_{clean} = 1$. To generate hadronic backgrounds, first we have calculated the realistic luminosity distribution of $\gamma\gamma$ collisions from beamstrahlung photons by a Monte Carlo simulation program CAIN. The luminosity distribution is described by two dimension of normalized cms energy $z = \sqrt{s}/(2E_e)$ and rapidity $\eta = \ln\sqrt{w_1/w_2}$ in order to take account of collisions between photons of unequal energy. Here $w_1$ and $w_2$ are the energies of left- and right-moving photons.

To represent the spatial distribution from minijet events, we use the parton distribution function of Drees and Grassie (DG-G) [27] for the photon by way of example. Because the saturation problem does not depend on the parameterizations of the photon density function as seen in the previous section. Here a cutoff $p_{t,min}$ for the DG-G parameterization in the previous section have been taken as

$$p_{t,min} = \begin{cases} 2.1 \ln\sqrt{s/21000}\ \text{GeV} & \sqrt{s} > 375\ \text{GeV} \\ 2.0\ \text{GeV} & \sqrt{s} \leq 375\ \text{GeV} \end{cases} \tag{9}$$

**TABLE 5.** The average visible energy and transverse momentum per event.

| Tracking Detector | | Calorimeters | |
|---|---|---|---|
| $E_{vis}$ (GeV) | $P_t$ (GeV) | $E_{vis}$ (GeV) | $P_t$ (GeV) |
| 6.6 | 4.0 | 34 | 13 |

where $s$ is given in $(\mathrm{GeV})^2$. Here the minimum of $p_{t,min}$ is assumed as 2.0 GeV, because we keep away from $p_{t,min} < 0$.

The subprocess cross sections in Eq.(6) have been calculated by using the PYTHIA 5.7 code. Subsequent hadronizations of minijets are simulated by the parton shower picture with the JETSET 7.3. In this analysis, the JLC-I detector simulator [33] is applied for selection performances in the JLC-I detector which has the acceptance $|\cos\theta| < 0.95$ [33]. The main components used in this simulator are the central drift chamber and calorimeters.

Figure 9 shows the distribution of the visible energy and the transverse momentum of the tracking detector and calorimeters. The number of generated events is 50000 and the event number in the histogram of Fig. 9 corresponds to an integrated luminosity of 0.1 $\mathrm{pb}^{-1}$. The 25% of all generated events are missed in the detector as shown by the peak. The deposits of the visible energy of the calorimeters are nearly below 200 GeV and the transverse momentum of the tracking detector above 40 GeV almost never has been seen.

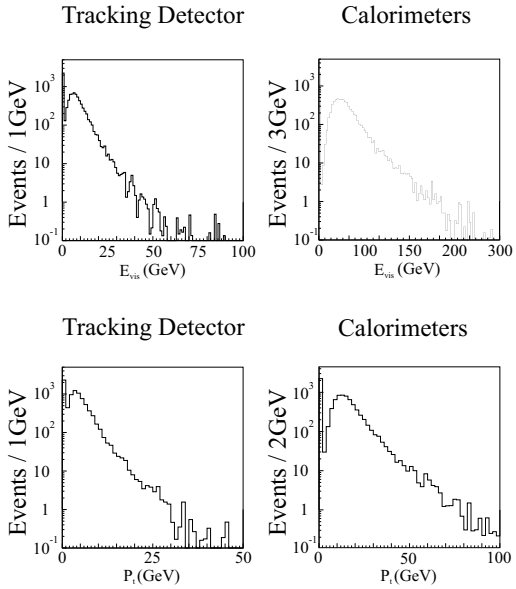


**FIGURE 9.** The distribution of the visible energy and the transverse momentum of the tracking detector and calorimeters. The number of events corresponds to an integrated luminosity of 0.1 $\mathrm{pb}^{-1}$.

The average visible energy and transverse momentum of the tracking detector and calorimeters per event are listed in Table 5. The energy deposits per event are more smaller than the 5 TeV collision energy of initial electron and positron beams. The simulation results on hadronic backgrounds at the 0.5 and 1 TeV Next Linear Collider [10] presented small energy depositions which are similar to our results. Since the particles from minijets will deposit most of their energy inside the mask. According to the table, it is shown that the selection by applying the cut of the visible energy and the transverse momentum greatly reduces the hadronic backgrounds.

# V CONCLUSION

We have estimated hadronic backgrounds by $\gamma\gamma$ collisions in an $e^+e^-$ collider at a center-of-mass energy of 5 TeV. The $e^+e^-$ linear collier based on the laser driven acceleration is adopted taking advantage of effects of quantum suppression of beamstrahlung. The assumption that the behavior of the total cross section of $\gamma\gamma$ collisions is similar to that of hadronic interactions at high energy is applied, because the assumption gives a reasonable description of the total cross section for $\gamma\gamma$ collisions as compared with experimental data. The number of hadronic backgrounds per bunch crossing is small so that it will not affect the performance of the detection in a study of elementary particle physics. Further we need to estimate the number of hadronic backgrounds taking account of the bunch scheme of the laser-driven linear colliders.

We have calculated the total cross sections of $\gamma\gamma$ minijets depended on the parton density function of the photon with the fixed minimum of transverse momentum and the results show the ambiguities on minijet cross sections at higher energy, related to the cutoff of transverse momentum. Therefore we propose the simple model for minijets by taking a phenomenological approach.

First, the simple ansatz that the total cross section of $\gamma\gamma$ minijets is supposed as that for $\gamma\gamma$ collisions, $\sigma_{\gamma\gamma} = (\sigma_{\gamma p})^2/\sigma_{pp}$, is applied as the upper bound of the minijet cross section. In order to evaluate the spatial distribution from minijet events, first we have calculated the fitting functions of the minimum transverse momentum, $p_{t,min}(\sqrt{s})$, which are depended on the photon parton distributions DG-G, LAC-1, GS-G, GRV-G, AFG-G, and SaS 2M by the PDFLIB 7.09 code on the assumption of the ansatz.

By using the fitting function of the minimum transverse momentum on the DG-G parameterization, we have performed the detector simulation. The detailed information of the minijets from realistic simulations is used to remove the hadronic backgrounds effectively. The Monte Carlo programs CAIN, PYTHIA 5.7, JETSET 7.3, and JLC-I detector simulator are applied for a 2-dimensional luminosity distribution of $\gamma\gamma$ collisions, the cross section of $\gamma\gamma$ minijets, hadronizations and selection performances in the detector, respectively. The results show that the energy deposits per event are more smaller than the 5 TeV collision energy of the

initial electron and positron beams.

## ACKNOWLEDGMENTS

We thank K. Yokoya for help on using the simulation code. We are grateful to J. Siegrist for making available the computer facility. T.O. thanks T. Tauchi for useful comments and discussions. This work was supported in part of the U.S. Department of Energy under Contract No. DE-AC03-76SF00098, and in part by the Grant-in-Aid for Scientific Research from Ministry of Education, Science and Culture of Japan.

## REFERENCES

1. T. Tauchi and H. Hayashii, in *Proc. of the Workshop on Physics and Experiments with Linear $e^+e^-$ Colliders*, Waikoloa, Hawaii, 26-30 April 1993, p.745
2. TOPAZ Collaboration, H. Hayashii *et al.*, Phys. Lett. B **314**, 149 (1993); AMY Collaboration, B.J. Kim *et al.*, Phys. Lett. B **325**, 248 (1994).
3. M. Drees and R.M. Godbole, Phys. Rev. Lett. **67**, 1189 (1991).
4. L3 Collaboration, M. Acciarri *et al.*, Phys. Lett. B **408**, 450 (1997).
5. F. Wäckerle, Talk given at *27th Int. Symposium on Multiparticle Dynamics*, INFN, Frascati, Italy, 1997; OPAL Collaboration, S. Söldner-Rembold *et al.*, Talk given at *18th Int. Symposium on Lepton-Photon Interactions*, Hamburg, Germany, 1997.
6. R.M. Godbole, in *Proc. of the 15th ICFA Advanced Beam Dynamics Workshop on Quantum Aspects of Beam Physics*, Monterey, CA, 4-9 Jan 1998.
7. T. Ohgaki, in *Proc. of the 15th ICFA Advanced Beam Dynamics Workshop on Quantum Aspects of Beam Physics*, Monterey, CA, 4-9 Jan 1998.
8. R.M. Barnett *et al.*, Phys. Rev. D **54**, 1 (1996).
9. A. Donnachie and P.V. Landshoff, Phys. Lett. B **296**, 227 (1992).
10. P. Chen, T.L. Barklow, and M.E. Peskin, Phys. Rev. D **49**, 3209 (1994).
11. M.M. Block, E.M. Gregores, F. Halzen, and G. Pancheri, Phys. Rev. D **58**, 017503 (1998).
12. R. Engel and J. Ranft, Phys. Rev. D **54**, 4244 (1996).
13. M. Xie, T. Tajima, K. Yokoya, and S. Chattopadhyay, in *Proc. of the 7th Workshop on Advanced Accelerator Concepts*, Lake Tahoe, CA, 13-19 Oct 1996.
14. M. Xie, in *Proc. of the 15th ICFA Advanced Beam Dynamics Workshop on Quantum Aspects of Beam Physics*, Monterey, CA, 4-9 Jan 1998.
15. K. Yokoya and P. Chen, in *Frontiers of Particle Beams: Intensity Limitations, Lecture Notes* in Physics Vol. 400 (Springer-Verlag, Berlin, 1992).
16. R.J. Noble, Nucl. Instrum. and Methods Phys. Res. A **256**, 427 (1987).
17. P. Chen, T. Ohgaki, A. Spitkovsky, T. Takahashi, and K. Yokoya, Nucl. Instrum. and Methods Phys. Res. A **397**, 458 (1997).

18. PLUTO Collaboration, Ch. Berger *et al.*, Phys. Lett. **149B**, 421 (1984) ; TPC/2$\gamma$ Collaboration, H. Aihara *et al.*, Phys. Rev. D **41**, 2667 (1990) ; MD1 Collaboration, S.E. Baru *et al.*, Z. Phys. C **53**, 219 (1992).
19. P.A. Baikov *et al.*, in *Proc. of 10th Int. Workshop on High-energy Physics and Quantum Field Theory*, Russia, 1995, p.101.
20. MINAMI-TATEYA group, T. Ishikawa *et al.*, KEK Report 92-19, 1993.
21. S. Chattopadhyay *et al.*, in *Proc. of the 1996 DPF/DPB Summer Study on New Directions for High-Energy Physics* (Snowmass 96), Snowmass, CO, 25 June - 12 July 1996.
22. G.A. Schuler and T. Sjöstrand, Z. Phys. C **73**, 677 (1997).
23. M. Drees and F. Halzen, Phys. Rev. Lett. **61**, 275 (1988).
24. M. Drees and R.M. Godbole, J. Phys. G **21**, 1559 (1995).
25. H. Plothow-Besch,"*PDFLIB: Structure Functions and $\alpha_s$ Calculations*", Users's Manual - Version 7.09, W5051 PDFLIB, 1997.07.02, CERN-PPE.
26. T. Sjöstrand, Comput. Phys. Commun. **82**, 74 (1994).
27. M. Drees and K. Grassie, Z. Phys. C **28**, 451 (1985).
28. H. Abramowicz, K. Charcula, and A. Levy, Phys. Lett. B **269**, 458 (1991).
29. P. Aurenche, J.P. Guillet, and M. Fontannaz, Z. Phys. C **64**, 621 (1994).
30. L.E. Gordon and J.K. Storrow, Nucl. Phys. B **489**, 405 (1997).
31. G.A. Schuler and T. Sjöstrand, Z. Phys. C **68**, 607 (1995).
32. M. Glück, E. Reya, and A. Vogt, Phys. Rev. D **46**, 1973 (1992).
33. "*JLC-I*", KEK Report 92-16, 1992.